Graphene quantum dots rescue angiogenic retinopathy via blocking STAT3/Periostin/ERK signaling

Na Zhao
Department of Ophthalmology, Shanghai Changhai Hospital, Naval Medical University
Xiao Gui
Department of Ophthalmology, Shanghai Changhai Hospital, Naval Medical University
Qian Fang
National Key Laboratory of Medical Immunology and Institute of Immunology, Naval Medical University
Rui Zhang
Department of Ophthalmology, Shanghai Changhai Hospital, Naval Medical University
Weiye Zhu
Department of Ophthalmology, Shanghai Changhai Hospital, Naval Medical University
Haorui Zhang
Department of Ophthalmology, Shanghai Changhai Hospital, Naval Medical University
Qing Li
Department of Ophthalmology, Shanghai Changhai Hospital, Naval Medical University
Yukun Zhou
Department of Ophthalmology, Shanghai Changhai Hospital, Naval Medical University
Jiawei Zhao
Department of Ophthalmology, Shanghai Changhai Hospital, Naval Medical University
Xiao Cui
Department of Ophthalmology, Shanghai Changhai Hospital, Naval Medical University
Guangping Gao
Department of Ophthalmology, Shanghai Changhai Hospital, Naval Medical University
Huipeng Tang
Department of Ophthalmology, Shanghai Changhai Hospital, Naval Medical University
Ni Shen
Department of Ophthalmology, Shanghai Changhai Hospital, Naval Medical University
Taoyong Chen
National Key Laboratory of Medical Immunology and Institute of Immunology, Naval Medical University
Hongyuan Song (hongyuansong@hotmail.com)
Department of Ophthalmology, Shanghai Changhai Hospital, Naval Medical University
Wei Shen

Department of Ophthalmology, Shanghai Changhai Hospital, Naval Medical University

Research Article

Keywords: retinal neovascularization, oxygen induced retinopathy, graphene quantum dots, periostin, cell cycle, RNA sequencing

Posted Date: February 11th, 2022

DOI: https://doi.org/10.21203/rs.3.rs-1329363/v1

Version of Record: A version of this preprint was published at Journal of Nanobiotechnology on April 2nd, 2022. See the published version at https://doi.org/10.1186/s12951-022-01362-4.

Abstract

Background: Pathological retinal angiogenesis resulting from a variety of ocular diseases including oxygen induced retinopathy, diabetic retinopathy and ocular vein occlusion, is one of the major reasons for vision loss, yet the therapeutic option is limited. Multiple nanoparticles have been reported to alleviate angiogenic retinopathy. However, the adverse effect cannot be ignored due to the relatively large scale. Graphene quantum dots (GQDs) have shown potential in drug delivery and have been proved biocompatible. In this study, Graphene quantum dots are extensively investigated for their application in angiogenic retinopathy therapy.

Results: We showed that GQDs were biocompatible nanomaterials *in vitro* and *in vivo*. The nanoparticles have a dose-dependent inhibitory effect on proliferation, migration, tube formation and sprouting of human umbilical vein endothelial cells (HUVECs). Further data show that GQDs could inhibit pathological retinal neovascularization in an oxygen-induced retinopathy (OIR) model. The data of RNA sequencing suggested that periostin is involved in this process. GQDs inhibit the expression of periostin via STAT3, and further regulated cell cycle-related protein levels through ERK pathway. The signaling pathway was conformed *in vivo* using OIR mouse model.

Conclusions: The present study indicated that GQDs could be a biocompatible anti-angiogenic nanomedicine in the treatment of pathological retinal neovascularization via disrupting periostin/ERK pathway and subsequent cell cycle.

Background

Diabetic retinopathy, retinopathy of prematurity and central retinal vein occlusion share the common pathological process named pathological retinal neovascularization, which is the major cause of severe vision loss and even blindness nowadays [1]. Current treatments for retinal neovascular diseases include laser photocoagulation, vitrectomy and intravitreal injection of cortisol or anti-VEGF therapy etc[2]. However, they are far from satisfaction, as decreased visual sensitivity, vitreous hemorrhage and retinal detachment often occur [3, 4]. So far, debate continues about the strategies for the management of retinal neovascularization related diseases. Hence, there remains a demand for exploring novel approaches for pathological retinal neovascularization.

Over the last few decades, nanomaterials are extensively researched, and nanotechnology has been applied extensively in biology, medicine, electronic engineering and other fields [5, 6]. It has been reported that nanomaterials have significant impact on angiogenesis due to their small size, high reactivity, and large surface area, including metal nanomaterials, silica-based nanomaterials and carbon-based nanomaterials [7]. Nowadays, carbon-based nanomaterials show great potential in nanomedicine for their unique chemical and physical properties, including carbon nanodots, carbon nanotubes, graphene, fullerenes, multi-walled carbon nanotube and carbon nanofibers [8-11]. Graphene, a new two-dimensional

carbon nanomaterial, is highly biocompatible and shows excellent stability, which is considered as a novel and promising nanomedicine [12, 13].

Different from conventional graphene oxide, graphene quantum dots (GQDs) are a novel nanomaterial made from few-layer graphene sheets (below 20 nm), which show wider application compared with graphene or graphene oxide (GO) [14, 15]. GQDs are able to penetrate through biological membranes and exhibit excellent biocompatibility, fluorescence properties, and superior physiological stability, which attract extensive interest within the field of bioimaging and targeted drug delivery [16, 17]. Furthermore, recent evidence suggests that GQDs exert a direct anti-tumor efficacy toward breast cancer *in vitro* and *in vivo*.[18] [19] Also, it is reported that GQDs could penetrate the blood brain barrier (BBB) and have an inhibitory effect on fibrillization of α-syn, triggering fibril disaggregation in Parkinson's disease [20] [21]. Pathological retinal angiogenesis shares some similarity with tumor such as uncontrolled cell growth and cell migration. Meanwhile, there is blood ocular barrier to avoid toxic substances. The previous investigations indicate that GQDs are able to penetrate BBB and suppress tumor growth, which indicates GQDs possess the potential to overcome the blood ocular barrier and to disrupt pathological retinal angiogenesis.

Periostin is a secreted matricellular protein, as well as an extracellular matrix (ECM) protein. It plays important roles in the development of bones, skins and heart, and involves in pathogenesis of various inflammatory diseases and tumor metastasis [22, 23]. Study shows that periostin is associated with the progression of hepatocellular carcinoma and it could activate hepatic stellate cells through integrin–FAK–STAT3–periostin pathway [24]. In the present study, we found that GQDs could inhibit angiogenesis *in vitro* and *in vivo*, and the transcriptomic analysis showed that RNA level of periostin and cell cycle-related proteins were different expressed in GQDs group. Western blotting demonstrated that the expression of periostin and cell cycle-related proteins was decreased after treatment by GQDs. GQDs inhibit the expression of periostin via STAT3, and further regulated cell cycle-related protein levels through ERK pathway. The signaling pathway was conformed *in vivo* using OIR mouse model. These data suggested that GQDs could be a novel anti-angiogenic drug for the treatment of pathological retinal angiogenesis.

Results

Characterization of GQDs

GQDs were purchased from Nanjing XFNANO Materials Tech Co Ltd (XF152, Nanjing, China). The microstructure of GQDs were characterized using TEM microscope. The GQDs were uniformly dispersed and showed spherical morphology **(Fig. 1A, 1B)**. As shown in **Fig. 1C**, the size distribution of GQDs ranged from 1 to 7 nm and the mean is 3.6 nm.

The effect of GQDs on cell proliferation

The biocompatibility of GQDs is of great importance for subsequent experiments. Thus, we first assessed the viability of HUVECs during a 24 h incubation with GQDs at 0, 12.5, 25, 50, and 100 μg mL^{-1}. The viability of HUVECs with GQDs at 12.5μg mL^{-1} showed no significant difference compared with GQDs at 0μg mL^{-1}, while exposure of HUVECs to GQDs at 25, 50 and 100μg mL^{-1} could inhibited the growth of HUVECs dose-dependently **(Fig. S1A)**. GQDs at 25 and 50 μg mL^{-1} were chosen as the appropriate concentration for follow-up experiments. To further test the biocompatibility of GQDs, we performed cell live/dead assay. HUVECs were treated with GQDs for 24h, then stained with Calcein-AM (CAM) and Propidium Iodide (PI) **(Fig. S1B)**. The percentages of HUVECs stained by PI were 1.1%, 1.0% and 1.1% respectively, showing no statistical difference among these three groups. The data showed that 25 and 50 μg mL^{-1} GQDs did not induce apparent cell toxicity.

Furthermore, we conducted EdU assay to explore the effect of GQDs on cell proliferation **(Fig. 2A)**. HUVECs were treated with GQDs at 0, 25 and 50 μg mL^{-1} for 24h and then stained by EdU cell proliferation assay kit. The result showed that the percentage of EdU positive cells in 25 μg mL^{-1} GQDs group and 50 μg mL^{-1} GQDs group decreased dose-dependently compared with control group **(Fig. 2B)**. The data indicated inhibitory effect of GQDs on HUVECs cell proliferation.

GQDs impair cell migration of HUVECs

To explore whether GQDs affected the cell migration of HUVECs, a wound healing assay was performed. HUVECs were seeded in twenty-well plates and wounded by a sterile pipette tip. After cocultured with GQDs (0, 25 and 50 μg mL^{-1}) for 16 hours, the scratch region of HUVECs nearly disappeared in the control group under the microscope. In contrast, 25 μg mL^{-1} GQDs group and 50 μg mL^{-1} GQDs group still exhibited obvious wounds in a dose-dependent manner, suggesting that the migration of HUVECs was inhibited when exposed to a concentration gradient of GQDs **(Fig. 3A, B)**.

The changes in cytoskeleton assembly are critical for cell migration. Thus, we used phalloidin and α-tubulin antibodies to stain the cytoskeleton of HUVECs to observe whether GQDs affected the cytoskeleton of HUVECs **(Fig. 3C)**. Immunofluorescence confocal laser scanning microscopy images indicated that GQDs could impair cytoskeletal assembly in HUVECs, contributing to decreased migration of HUVECs. All together, these results demonstrated that GQDs could efficiently impair cell migration of HUVECs *in vitro*.

GQDs attenuate tube formation and sprouting of HUVECs

To evaluate the ability of GQDs to attenuate angiogenesis *in vitro*, we performed a tube formation assay on Matrigel. As shown in **Fig. 4A, B**, the number of capillary-like structures decreased apparently in GQDs treated groups than that in control group. To further verify the anti-angiogenic ability of GQDs *in vitro*, we analyzed HUVECs sprouting using the sprouting assay. The data showed that the ability of HUVECs to sprout was significantly attenuated by GQDs **(Fig. 4C-E)**. Taken together, the above cell function experiment showed that GQDs could inhibit endothelial cells angiogenesis *in vitro* dose-dependently.

GQDs inhibit retinal angiogenesis in the OIR model.

To further evaluate the effect of GQDs on angiogenesis *in vivo*, we established oxygen induced retinopathy model (OIR model), in which hyperoxia caused significant vessel loss and then room air caused hypoxic avascular retina to trigger normal blood vessels regeneration and retinal neovascularization. The retinas were collected and fixed at P17 and FITC-isolectin B4 (IB4) was used to stain retinal vessels to quantify the nonperfusion area and neovascular areas. The results showed that compared with normal retinal vasculature of mice, there were significant nonperfusion area and neovascular tufts in retina of OIR model **(Fig. 5A and Fig. 5C)**. Subsequently, we performed intravitreal injection with GQDs (1mg mL^{-1},2μL) and PBS (2μL) in OIR model at P12 respectively. The toxicity in vivo was evaluated by hematoxylin and eosin staining. The data indicated that GQDs were biocompatible *in vivo* **(Fig. S2)**. Then, the retinas were collected, fixed and stained as above. Notably, intravitreal injection with GQDs could significantly decrease nonperfusion area and neovascular areas of OIR mice compared with injection with PBS **(Fig. 5A-D)**, indicating GQDs could inhibit retinal neovascularization *in vivo* in OIR model.

Analysis of gene expression profiles in GQDs treated HUVECs

To further identify the mechanisms of GQDs inhibiting angiogenesis, we next performed RNA sequencing analysis of HUVECs in control and GQDs treated groups. Firstly, we calculated the Pearson correlation coefficient of data from three GQDs treated groups and three control groups, finding that significant differences existed in the correlations between GQDs groups and control groups **(Fig. 6A)**. A total of 16380 genes were identified, among which 1817 genes were screened to be differentially expressed in GQDs treated groups compared to control group (678upregulated genes and1139 downregulated genes) **(Fig. 6B and Fig. 6C)**. Periosin (postn) belongs to the top ten differentially expressed genes after treatment with GQDs **(Fig. 6D)**. Gene ontology (GO) analysis was implemented to analyze the function of the differently expressed genes. As shown in **Fig. 6E**, the genes were enriched for cell cycle process and cell cycle. Meanwhile, we performed pathway enrichment analysis of significant proteins through Kyoto Encyclopedia of Genes and Genomes (KEGG), finding that cell cycle was also involved in the major pathways **(Fig. 6E)**. Therefore, we proposed the assumption that periostin and cell cycle-related proteins were associated with the inhibitory effects of GQDs on angiogenesis.

GQDs induce cell cycle arrest in G1 phase

Generally, cell cycle can be divided into three phases, G0/G1 phase, S phase, and G2/M phase according to DNA synthesis [25]. Flow cytometry was used to analyze the cell cycle change of HUVECs after the cells were treated with GQDs for 24 h. As is showed in **Fig. 7A, B**, GQDs could significantly induce HUVECs cell cycle arrest at G1 phase with a decreased distribution in S phase. Sequential activation of cyclins and cyclin-dependent kinases is involved in the regulation of the cell cycle [26]. To verify whether the cell cycle-related proteins were involved in GQDs induced cell cycle arrest, we conducted western blotting. As revealed in **Fig. 7C**, the expression of CDK2, CYCLIN D1, CYCLIN E1 were decreased in GQDs treatment

groups compared to control. Minichromosome maintenance (MCM) proteins play an important role in promoting DNA replication [27]. We also found that GQDs could inhibit the expression of MCM5 and MCM7 in HUVECs **(Fig. 7C)**. Meanwhile, there was no differential expression of the apoptosis-associated proteins named caspase 3 **(Fig. 7C, D)**. Collectively, the results above suggested that GQDs effectively inhibited cell cycle progression via inducing cell cycle arrest at G1 phase by a reduction in the expression cell cycle-related proteins in HUVECs, while apoptosis-related protein was not affected.

GQDs inhibit the expression of periostin by downregulating p-STAT3

RNA sequencing analysis revealed the inhibited expression of preiostin in GQDs group compared with control group. Therefore, western blotting was performed to analyze the expression of periostin in GQDs treated HUVECs and control group. Consistent with the result of gene expression profiles, the level of periostin in GQDs treated groups decreased significantly, which suggested GQDs might inhibit retinal angiogenesis through suppressing the expression of periostin **(Fig. 8A-B)**. STAT3 is a transcription factor, which controls the expression of periostin[28]. Then, we analyzed the expression of p-STAT3 by western blotting. In line with the aforementioned studies, we found that a decreased expression of p-STAT3 following the treatment with GQDs **(Fig. 8A-B)**. Taken together. These data confirmed that STAT3-periostin signaling pathways was disrupted in the process of GQDs inhibiting angiogenesis.

Additionally, the results of immunofluorescence assay *in vivo* also supported the hypothesis. We first observed the expression of periostin in retinal vascular. The data showed that the expression of periostin co-localized with IB4 stained retinal blood vessels, and periostin was highly expressed in neovascular tufts in the OIR model **(Fig. S3A)**. The data suggested that periostin was up-regulated in the blood vessels in OIR model, which could be a target for intervention of pathological angiogenesis. After intravitreal injection of GQDs, the fluorescence signals of both p-STAT3 and periostin were decreased in neovascular areas compared with PBS groups **(Fig. 8C)**, which was consistent with the data *in vitro*. These data suggested that GQDs could inhibit angiogenesis by inhibiting STAT3- periostin signaling pathways *in vitro* and *in vivo*.

Previous studies indicated that there was a close association between periostin and cell cycle-related proteins. It was reported that periostin silencing down-regulated expression of cyclins E2, A2, CDK1, CDK 2, and CDK 6 though ERK pathway in lung fibroblasts [29]. Based on our gene sequencing analysis that Postn and cell cycle-related genes were differently expressed in GQDs group, we presented our hypothesis that periostin might control cell cycle via regulation of ERK pathway in GQDs group. Thus, we performed western blot analysis to quantify the expression of ERK pathway. The expression of p-ERK in HUVECs treated with GQDs was decreased **(Fig. 8D, E)**. Altogether, the data indicated that GQDs could inhibit angiogenesis *in vitro* and *vivo* by disrupting p-STAT3/periosin /p-ERK pathway and subsequent cell cycle.

Discussion

At present, laser photocoagulation and anti-VEGF intravitreal injection are the major Clinical treatments for retinal neovascularization, but there are still some defects. Finding an effective angiogenesis inhibitor

remains a subject of intensive research due to no completely safe and long-term effective treatment for retinal neovascularization currently. In previous study, our team have found that Gold Nanorods could suppress angiogenesis by affecting ECs cell division, and that cuprous oxide nanoparticles features anti-angiogenic agents through down regulating the expression of VEGFR2 [30, 31]. These findings showed the anti-angiogenic potentials of metal and metal oxide nanomaterials, yet the relatively larger particle size might lead to adverse effects. GQDs possess smaller size, exceptional physicochemical properties and high biocompatibility, which has received extensive attention in biomedical applications [32]. It is reported that GQDs could induce apoptosis and inflammatory response in macrophages by upregulating inflammation [33]. There are also studies revealing the potential of GQDs in photodynamic therapy for cancer treatment [15]. To our best knowledge, the anti-angiogenic role of GQDs has not been reported before. This is the first report demonstrated that GQDs could inhibit angiogenesis *in vitro* and *in vivo* through down-regulating periostin expression.

The biocompatibility of NPs was a prerequisite for the future clinical application. Recently studies have shown that many metal nanoparticles and metal oxides nanomaterials possess anti-angiogenesis activities [31, 34, 35]. Nevertheless, it is reported that metal nanoparticles and metal oxides nanomaterials have potential toxicity in cells or biology by causing oxidative stress, inflammation, genetic damage [36, 37]. GQDs, with lateral dimensions of less than 10 nm, is a novel nanomaterial with many advantages, such as good biocompatibility, high water solubility and photostability [15]. Experiments by Tanveer et al. demonstrated that GQDs have minimal toxicity to cells cultured *in vitro* and in vital organs of rats [38]. Given problems of biocompatibility, we performed cell live/dead assay, the results of which showed its safety in anti-angiogenic applications. Owing to their extreme small size, GQDs could penetrate the biological membranes and be cleared rapidly through the kidneys. Many researches proved that GQDs was a nanomaterial with low cytotoxicity *in vitro* and *in vivo* [16, 17]. GQDs can enter the cells very easily through caveolae-mediated endocytosis and tend to accumulate in ER and nucleus, due to their smaller lateral size. Compared with GO, GQDs induce less internal cellular reactive species (ROS) level and damage to mitochondrial membranes potential. That is the reason that GQDs are relatively easier to be untaken into cells but have lower cytotoxicity than GO sheets [39].

It is well known that the angiogenesis of ECs *in vitro* includes cell proliferation, migration, and ability to form capillary-like tube structure [40]. Our results of cell proliferation, cell migration assay, capillary-like tube formation and sprouting assay demonstrated that GQDs had significant anti-angiogenic potential *in vitro* in a dose-dependent manner. The OIR model is a classic model for studying pathological neovascularization after retinal ischemia [41]. We established OIR model to evaluate the effect of GQD on retinal neovascularization. There was a robust reduction of nonperfusion area and neovascular areas in the retina of mouse injected with GQDs compared with that of mouse injected with PBS, showing a significant inhibition of pathological retinal angiogenesis by GQDs.

Periostin, a secreted matricellular protein, plays a crucial role in cell proliferation, differentiation and migration [42]. Nowadays, studies revealed that periostin is associated with multiple cancers such as colon, pancreatic, ovarian, breast cancer [43]. Microarray analysis of gene expression of HUVECs treated

with GQDs revealed decreased expression of periostin, which may illustrate the underlying molecular mechanism of anti-angiogenic capacity of GQDs. The result of western blotting validated that the expression of periostin was downregulated in GQDs treated cells, which was consistent with the previous sequencing results. Several studies have reported that the expression of periosin was regulated by STAT3[28, 44]. Our data were consistent with these reports, revealing the molecular mechanisms that GQDs prevented angiogenesis *in vitro* and *in vivo* through suppressing STAT3/periostin pathway. Meanwhile, these results were further confirmed in an OIR model. In a classical OIR model, we observed that there was an increased expression of p-STAT3 and periostin in the peripheral neovascular tufts of retina. After an intravitreal injection of GQDs, the fluorescence intensity of p-STAT3 and periostin decreased significantly in neovascular areas. The data suggested that GQDs could suppress angiogenesis in an OIR model and downregulate of expression of p-STAT3 and periostin simultaneously. Thus, we proposed that the inhibition of retinal angiogenesis by GQDs was mediated through STAT3-periostin signaling pathway.

The cell cycle can be divided into three phases, G0/G1 phase, S phase, and G2/M phase according to DNA synthesis [25]. The EdU proliferation assay revealed that GQDs could inhibit the growth of HUVECs *in vitro* and RNA sequencing showed differential expression of both periostin and cell cycle-related genes. To further reveal the possible mechanism, we performed flow cytometric analysis which demonstrated that GQDs could induce cell cycle arrest at G1 phase in HUVECs. Western blotting suggested that the expression of cell cycle-related proteins was decreased in GQDs treated groups, including CDK2, Cyclin D1, Cyclin E1, MCM5 and MCM7. Meanwhile, there was no difference in the expression of caspase 3 which was known as a key executioner of apoptosis [45]. The data further proved the biocompatibility of GQDs. Altogether, these findings indicated that GQDs could inhibit cell proliferation via regulating cell-cycle progression. As described above, studies revealed that periostin could regulate cell cycle-related proteins expression via p-ERK signaling pathway. We analyzed the expression of p-ERK of HUVECs treated with GQDs and the results demonstrated that the expression of p-ERK was decreased in GQDs groups. Therefore, we concluded that GQDs could inhibit pathological retinal angiogenesis *in vitro* and *in vivo* by disrupting STAT/periosin/ERK pathway and subsequent cell cycle **(Figure 9)**.

Conclusions

In summary, we demonstrated that GQDs could inhibit the proliferation, migration, tube formation and sprouting of HUVECs *in vitr*o and improve pathological angiogenesis in a OIR model, which highlight the potential of GQDs as an angiogenesis inhibitor. GQDs suppressed periostin and cell cycle-related proteins expression, arresting cell cycle in the G1 phase. Furthermore, our study revealed the association between periostin and cell cycle-related proteins after treatment with GQDS. The decreased expression of periostin could inactivate the phosphorylation of ERK to regulate cell cycle-related proteins. These results suggested that GQDs could be a novel anti-angiogenic drug for the treatment of pathological retinal angiogenesis.

Methods

Materials

GQDs were purchased from Nanjing XFNANO Materials Tech Co Ltd (XF152, Nanjing, China). Antibodies to β-actin, Cyclin D1, Cyclin E1, CDK2 MCM5, MCM7, caspase 3, periostin, p-STAT were purchased from Proteintech Group (Wuhan, China). Horseradish peroxidase (HRP)- conjugated anti-mouse and anti-rabbit secondary antibodies were from Jackson ImmunoResearch (West Grove, PA, USA). Tublin, DAPI were purchased from ThermoFisher (Shanghai, China). Cell Counting Kit-8(CCK-8) was from Dojindo Laboratories, (Dojindo, Japan). Cell-light EdU Apollo567 In Vitro Kit was purchased from RiboBio (Guangzhou, China). Matrigel Matrix was purchase from BD Biosciences. (Shanghai, China). Isolectin B4 was purchased from Sigma-Aldrich (Shanghai, China). All of the cell culture plates were bought from Corning Life Sciences.

Cell culture

HUVECs were obtained from ScienCell (San Diego, USA) and cultured in Endothelial Cell Medium (ECM, Cell Research, Shanghai, China) supplemented with 5% FBS, 1% endothelial cells growth supplement (ECGS) and 1% penicillin-streptomycin in a humidified atmosphere with 5% CO2 and a temperature of 37 ◦C. The cells were seeded into indicated plates for different assays when growing to 80%-90% confluence.

Cytotoxicity assay for HUVECs

The cytotoxicity of the GQDs was evaluated by the CCK-8 assay. Cells were seeded in 96-well plates at a density of 2.0×10^3 cells per well and cultured in the conditions as above for 6h. GQDs were added to the wells and cultured with the cells for 24 h. Then, the original medium was removed and 100 μL of the CCK-8 solution (10 μL CCK-8 in 90 μL ECM) was added each well and incubated for an additional 2 h. The absorbance of CCK-8 was measured by a microplate reader at a test wavelength of 450 nm with a reference wavelength of 690 nm. Cell viability (%) was equal to (OD450test − OD450blank)/(OD450control − OD450blank) × 100%. All experiments were repeated three times with three duplications.

Cell proliferation assay

Cellular proliferation rate was measured by 5-ethynyl-2-deoxyuridine (EdU) assays as we described previously. In short, cells were seeded at a density of 2.0×10^3 cells per well in 96-well plates and incubated overnight. GQDs were added into wells and incubate for 24 hours. Then the culture medium was replaced with 100 uL fresh medium along with EdU (100 mM). After incubation for 2 h, the cells were stained according to the following protocol: the EdU medium was poured off and then the cells were fixed with 4% paraformaldehyde for 30 minutes. Then, glycine was added to wash cells for 5 minutes, followed by twice washes with 0.2% Trion X-100 of 100uL. Subsequently, 100 μL of Apollo fluorescent azide was added to each well to stain cells and incubated in the dark for 30 min, followed by three washes with 0.2%

Trion X-100 of 100uL. Finally, Hoechst was added for another 30min and then cells were washed with PBS three times and kept in PBS until imaging. The images were acquired and analyzed using a digital microscope system (IX81, Olympus).

Cell migration assay

5×10^5 HUVECs were added to 12-well plate and cultured with medium overnight. Scratch wounds were created across the surface of the plates using a sterile 200-μl pipette tip and the medium containing suspension cells were removed and cells were rinsed with PBS for 3 times. GQDs were added into the wells and cultured at 37 degrees with 5% CO2. 16 h later, cells were fixed with paraformaldehyde (4% in PBS) for 10 min at room temperature and subsequently washed twice with PBS. Finally, samples were observed through microscope (IX81, Olympus).

Tube formation assay

These assays were conducted following the instructions provided by the manufacturer. Firstly, Matrigel was melted at 4 °C overnight and diluted with serum-free medium. 90 μLdiluted Matrigel was added to each well of 96-well plate and solidified at 37 °C for 40 min. Then, HUVECs treated with 25 and 50μg mL^{-1} GQDs for 24 h were digested by trypsin and then 2×10^4cells were gently added to each Matrigel-coated well and incubated at 37 °C for 3 h. Images were captured using an Olympus IX81 microscope.

Cell cycle assay

HUVECs were seeded in a 6-well plate and incubated overnight and then starved for 16 hours. Subsequently, starved cells were treated with 25 and 50μg mL^{-1} GQDs for another 72 hours and then cells were trypsinized, washed twice in PBS and fixed overnight in 70% ethanol at 4°C. The next day ethanol was removed by centrifugation and cells were washed twice with cold PBS. Finally, cells were resuspended in PBS containing ribonuclease (200 μg/ml) and propidium iodide (20 μg/ml) and incubated for 30 min. The samples were immediately analyzed by Cell Lab Quanta SC flow cytometer (BECKMAN COULTER) and data were analyzed using ModFit software.

Western blot analysis

Total proteins of HUVECs in 6-well plates were extracted using RIPA lysis buffer (Beyotime, Shanghai, China) supplemented with protease inhibitors (20 uL/mL) and phosphatase inhibitors (20 uL/mL). Then proteins (20ul samples per lane) were separated on 10% polyacrylamide gels by SDS-PAGE and transferred onto PVDF membranes. After blocked with 5% skimmed milk for 1h

at room temperature, the blots were incubated with various concentrations of primary antibodies at 4°C overnight according to the manufacturer's protocols. Then the membranes were washed three times in TBS-T for 5 min each time and subsequently incubated with horseradish peroxidase–conjugated goat anti-mouse or anti-rabbit antibodies (1:10,000 dilution) for 2 hours, followed by three washes with TBS-T

5 to 7 min each time. Lastly, the blots incubated with ECL Super Signal West Pico Chemiluminescent Substrate (Thermo Scientific) and detected using the GeneGnome HR Image Capture System (Syngene).

Gene expression microarrays

Cells in culture dishes were treated with 50μg mL^{-1} GQDs for 24 hours and then lysed using Trizol reagent (Invitrogen) to collect total RNA. The samples were submitted to Beijing Genomics institution (Beijing, China) for mRNA sequencing and analysis. Differentially expressed mRNAs were identified by fold-change filtering (fold change >2). Heatmaps were generated by Hierarchical Clustering with average linkage in Cluster 3.0 and visualized using Java TreeView program. Subsequently, the standard enrichment computation method was used to perform GO and KEGG pathway analyses.

Retina Preparation and Analyses

The oxygen induced retinopathy (OIR) model was induced to analyze retinal angiogenesis as previously described [30]. From P7 to P12, pups and their nursing mothers were exposed to 75% oxygen and on P12 the pups were removed from oxygen supply chamber and randomly divided into two groups: GQDs-treated group and control group. 12-day-old pups were intravitreally injected with GQDs (1mg/mL,2μL) in right eye using a 5-μL Hamilton syringe equipped with 50-gage glass capillary, and PBS (2μL) in the contralateral eye. Five days later, the mice were euthanized by inhalation of CO_2 and their eyes were enucleated and then fixed in 4% paraformaldehyde overnight at 4°C. Hereafter, retinas were isolated in their entirety under a microscope and then block with 1% BSA and 0.3% Triton X-100 for 30 min at room temperature. After three times wash in PBS, the retinas were stained with FITC- conjugated Isolectin B4 and indicated primary antibody overnight at 4°C. Then retinas were washed three times with PBS and incubated with FITC-labelled secondary antibody for 2h at room temperature. After that, the samples were washed with PBS two times and counter-stained with DAPI (1:2000) in PBS for 30min, followed by three PBS washes. Finally, retinas were carefully flat mounted onto glass slides and sealed with resinene. Slides were photographed using Leica TCS SP5-II confocal microscope system and the avascular areas and neovascular areas were quantified using Image J software.

Statistical analysis

Each experiment was carried out in triplicates, and repeated at least three times. The data were first tested for normality using SPSS software (SPSS 18.0 software) and then analyzed by one-way ANOVA using Prism software (GraphPad 9.0). All results were presented as a mean ± standard deviation (SD) and the statistical differences between two groups were analyzed by unpaired Student's t-test with statistical significance assumed at $P < 0.05$.

Abbreviations

OIR: Oxygen induced retinopathy

GQDs: Graphene quantum dots

HUVECs: Human umbilical vein endothelial cells

BBB: Blood brain barrier

TEM: Transmission electron microscope

CAM: Calcein-AM

PI: Propidium Iodide

IB4: isolectin B4

GO: Gene ontology

KEGG: Kyoto Encyclopedia of Genes and Genomes

EdU: 5-ethynyl-2-deoxyuridine

Declarations

Author Contributions

HYS and WS conceived and designed the project. NZ, XG, QF and HRZ performed the experiments *in vitro*. WYZ, JWZ, XC, GPG and HPT contributed to the analyze and summarize the data. NZ, YKZ, and RZ write the original draft. QL, WYZ and NS perform the *in vivo* experiment. TYC and WS drafted and revised the manuscript. All authors have read and agreed to the published version of the manuscript.

Consent for publication

All the authors agree with the publication.

Availability of Data and materials

All data used to support the findings of this study are included within the article.

Funding

This research was supported by the National Natural Science Foundation of China (82171081, 81800624, 81700839), Shanghai Pujiang Program (21PD068), China Postdoctoral Science Foundation (2018M632122) and “Chen Guang” project supported by the Shanghai Municipal Education Commission, and the Shanghai Education Development Foundation (18CG40).

Ethics approval and consent to participate

Not applicable.

Competing interests

The authors declare no competing interests.

References

1. Selvam S, Kumar T, Fruttiger M: Retinal vasculature development in health and disease. *Prog Retin Eye Res* 2018, 63:1-19.

2. Tsai ASH, Cheung N, Gan ATL, Jaffe GJ, Sivaprasad S, Wong TY, Cheung CMG: Retinal angiomatous proliferation. *Surv Ophthalmol* 2017, 62(4):462-492.

3. Liao ZY, Liang IC, Li HJ, Wu CC, Lo HM, Chang DC, Hung CF: Chrysin Inhibits High Glucose-Induced Migration on Chorioretinal Endothelial Cells via VEGF and VEGFR Down-Regulation. *Int J Mol Sci* 2020, 21(15).

4. Hanna RM, Barsoum M, Arman F, Selamet U, Hasnain H, Kurtz I: Nephrotoxicity induced by intravitreal vascular endothelial growth factor inhibitors: emerging evidence. *Kidney international* 2019, 96(3):572-580.

5. Chen J, Ning C, Zhou Z, Yu P, Zhu Y, Tan G, Mao C: Nanomaterials as photothermal therapeutic agents. *Prog Mater Sci* 2019, 99:1-26.

6. Fischer J, Beckers SJ, Yiamsawas D, Thines E, Landfester K, Wurm FR: Targeted Drug Delivery in Plants: Enzyme-Responsive Lignin Nanocarriers for the Curative Treatment of the Worldwide Grapevine Trunk Disease Esca. *Adv Sci (Weinh)* 2019, 6(15):1802315.

7. Kargozar S, Baino F, Hamzehlou S, Hamblin MR, Mozafari M: Nanotechnology for angiogenesis: opportunities and challenges. *Chem Soc Rev* 2020, 49(14):5008-5057.

8. Karousis N, Suarez-Martinez I, Ewels CP, Tagmatarchis N: Structure, Properties, Functionalization, and Applications of Carbon Nanohorns. *Chem Rev* 2016, 116(8):4850-4883.

9. Mukherjee S, Patra CR: Therapeutic application of anti-angiogenic nanomaterials in cancers. *Nanoscale* 2016, 8(25):12444-12470.

10. Su Y, Hu Y, Wang Y, Xu X, Yuan Y, Li Y, Wang Z, Chen K, Zhang F, Ding X *et al*: A precision-guided MWNT mediated reawakening the sunk synergy in RAS for anti-angiogenesis lung cancer therapy. *Biomaterials* 2017, 139:75-90.

11. Xin Q, Shah H, Nawaz A, Xie W, Akram MZ, Batool A, Tian L, Jan SU, Boddula R, Guo B *et al*: Antibacterial Carbon-Based Nanomaterials. *Adv Mater* 2019, 31(45):e1804838.

12. Fong YT, Chen CH, Chen JP: Intratumoral Delivery of Doxorubicin on Folate-Conjugated Graphene Oxide by In-Situ Forming Thermo-Sensitive Hydrogel for Breast Cancer Therapy. *Nanomaterials (Basel)* 2017, 7(11).

13. Tabish TA: Graphene-based materials: The missing piece in nanomedicine? *Biochemical and biophysical research communications* 2018, 504(4):686-689.

14. Du Y, Guo S: Chemically doped fluorescent carbon and graphene quantum dots for bioimaging, sensor, catalytic and photoelectronic applications. *Nanoscale* 2016, 8(5):2532-2543.

15. Fan HY, Yu XH, Wang K, Yin YJ, Tang YJ, Tang YL, Liang XH: Graphene quantum dots (GQDs)-based nanomaterials for improving photodynamic therapy in cancer treatment. *Eur J Med Chem* 2019, 182:111620.

16. Henna TK, Pramod K: Graphene quantum dots redefine nanobiomedicine. *Mater Sci Eng C Mater Biol Appl* 2020, 110:110651.

17. Lu H, Li W, Dong H, Wei M: Graphene Quantum Dots for Optical Bioimaging. *Small* 2019, 15(36):e1902136.

18. Ge J, Lan M, Zhou B, Liu W, Guo L, Wang H, Jia Q, Niu G, Huang X, Zhou H *et al*: A graphene quantum dot photodynamic therapy agent with high singlet oxygen generation. *Nat Commun* 2014, 5:4596.

19. Yousaf M, Huang H, Li P, Wang C, Yang Y: Fluorine Functionalized Graphene Quantum Dots as Inhibitor against hIAPP Amyloid Aggregation. *ACS Chem Neurosci* 2017, 8(6):1368-1377.

20. Kim D, Yoo JM, Hwang H, Lee J, Lee SH, Yun SP, Park MJ, Lee M, Choi S, Kwon SH *et al*: Graphene quantum dots prevent α-synucleinopathy in Parkinson's disease. *Nat Nanotechnol* 2018, 13(9):812-818.

21. Lai PX, Chen CW, Wei SC, Lin TY, Jian HJ, Lai IP, Mao JY, Hsu PH, Lin HJ, Tzou WS *et al*: Ultrastrong trapping of VEGF by graphene oxide: Anti-angiogenesis application. *Biomaterials* 2016, 109:12-22.

22. Duchamp de Lageneste O, Julien A, Abou-Khalil R, Frangi G, Carvalho C, Cagnard N, Cordier C, Conway SJ, Colnot C: Periosteum contains skeletal stem cells with high bone regenerative potential controlled by Periostin. *Nat Commun* 2018, 9(1):773.

23. Ma H, Wang J, Zhao X, Wu T, Huang Z, Chen D, Liu Y, Ouyang G: Periostin Promotes Colorectal Tumorigenesis through Integrin-FAK-Src Pathway-Mediated YAP/TAZ Activation. *Cell Rep* 2020, 30(3):793-806.e796.

24. Xiao H, Zhang Y, Li Z, Liu B, Cui D, Liu F, Chen D, Liu Y, Ouyang G: Periostin deficiency reduces diethylnitrosamine-induced liver cancer in mice by decreasing hepatic stellate cell activation and cancer cell proliferation. *The Journal of Pathology* 2021, 255(2):212-223.

25. Li XY, Wang DP, Lu GQ, Liu KL, Zhang TJ, Li S, Mohamed OK, Xue WH, Qian XH, Meng FH: Development of a novel thymidylate synthase (TS) inhibitor capable of up-regulating P53 expression and inhibiting angiogenesis in NSCLC. *J Adv Res* 2020, 26:95-110.

26. Icard P, Fournel L, Wu Z, Alifano M, Lincet H: Interconnection between Metabolism and Cell Cycle in Cancer. *Trends Biochem Sci* 2019, 44(6):490-501.

27. Casar Tena T, Maerz LD, Szafranski K, Groth M, Blätte TJ, Donow C, Matysik S, Walther P, Jeggo PA, Burkhalter MD *et al*: Resting cells rely on the DNA helicase component MCM2 to build cilia. *Nucleic Acids Res* 2019, 47(1):134-151.

28. Amara S, Lopez K, Banan B, Brown SK, Whalen M, Myles E, Ivy MT, Johnson T, Schey KL, Tiriveedhi V: Synergistic effect of pro-inflammatory TNFα and IL-17 in periostin mediated collagen deposition: potential role in liver fibrosis. *Mol Immunol* 2015, 64(1):26-35.

29. Yoshihara T, Nanri Y, Nunomura S, Yamaguchi Y, Feghali-Bostwick C, Ajito K, Murakami S, Mawatari M, Izuhara K: Periostin plays a critical role in the cell cycle in lung fibroblasts. *Respir Res* 2020, 21(1):38.

30. Song H, Guo T, Zhao Z, Wei Y, Luo H, Weng W, Zhang R, Zhong M, Chen C, Su J *et al*: Biocompatible PEGylated Gold nanorods function As cytokinesis inhibitors to suppress angiogenesis. *Biomaterials* 2018, 178:23-35.

31. Song H, Wang W, Zhao P, Qi Z, Zhao S: Cuprous oxide nanoparticles inhibit angiogenesis via down regulation of VEGFR2 expression. *Nanoscale* 2014, 6(6):3206-3216.

32. Drissi L, Ouarrad H, Ramadan F, Fritzsche W: Graphene and silicene quantum dots for nanomedical diagnostics. *RSC Advances* 2020, 10(2):801-811.

33. Qin Y, Zhou ZW, Pan ST, He ZX, Zhang X, Qiu JX, Duan W, Yang T, Zhou SF: Graphene quantum dots induce apoptosis, autophagy, and inflammatory response via p38 mitogen-activated protein kinase and nuclear factor-κB mediated signaling pathways in activated THP-1 macrophages. *Toxicology* 2015, 327:62-76.

34. Singh R, Batoki JC, Ali M, Bonilha VL, Anand-Apte B: Inhibition of choroidal neovascularization by systemic delivery of gold nanoparticles. *Nanomedicine* 2020, 28:102205.

35. Yang T, Yao Q, Cao F, Liu Q, Liu B, Wang XH: Silver nanoparticles inhibit the function of hypoxia-inducible factor-1 and target genes: insight into the cytotoxicity and antiangiogenesis. *Int J Nanomedicine* 2016, 11:6679-6692.

36. Hu X, Sun A, Kang W, Zhou Q: Strategies and knowledge gaps for improving nanomaterial biocompatibility. *Environ Int* 2017, 102:177-189.

37. Zhu Y, Wu J, Chen M, Liu X, Xiong Y, Wang Y, Feng T, Kang S, Wang X: Recent advances in the biotoxicity of metal oxide nanoparticles: Impacts on plants, animals and microorganisms. *Chemosphere* 2019, 237:124403.

38. Tabish TA, Scotton CJ, Ferguson DCJ, Lin L, der Veen AV, Lowry S, Ali M, Jabeen F, Ali M, Winyard PG *et al*: Biocompatibility and toxicity of graphene quantum dots for potential application in photodynamic therapy. *Nanomedicine (Lond)* 2018, 13(15):1923-1937.

39. Wu C, Wang C, Han T, Zhou X, Guo S, Zhang J: Insight into the cellular internalization and cytotoxicity of graphene quantum dots. *Adv Healthc Mater* 2013, 2(12):1613-1619.

40. Eelen G, Treps L, Li X, Carmeliet P: Basic and therapeutic aspects of angiogenesis updated. *Circulation research* 2020, 127(2):310-329.

41. Rohlenova K, Goveia J, García-Caballero M, Subramanian A, Kalucka J, Treps L, Falkenberg KD, de Rooij LP, Zheng Y, Lin L: Single-cell RNA sequencing maps endothelial metabolic plasticity in pathological angiogenesis. *Cell metabolism* 2020, 31(4):862-877. e814.

42. Kudo A, Kii I: Periostin function in communication with extracellular matrices. *Journal of cell communication and signaling* 2018, 12(1):301-308.

43. González-González L, Alonso J: Periostin: a matricellular protein with multiple functions in cancer development and progression. *Frontiers in oncology* 2018, 8:225.

44. Mishra SK, Wheeler JJ, Pitake S, Ding H, Jiang C, Fukuyama T, Paps JS, Ralph P, Coyne J, Parkington M *et al*: Periostin Activation of Integrin Receptors on Sensory Neurons Induces Allergic Itch. *Cell Rep* 2020, 31(1):107472.

45. Huang Q, Li F, Liu X, Li W, Shi W, Liu FF, O'Sullivan B, He Z, Peng Y, Tan AC *et al*: Caspase 3-mediated stimulation of tumor cell repopulation during cancer radiotherapy. *Nat Med* 2011, 17(7):860-866.

Figures

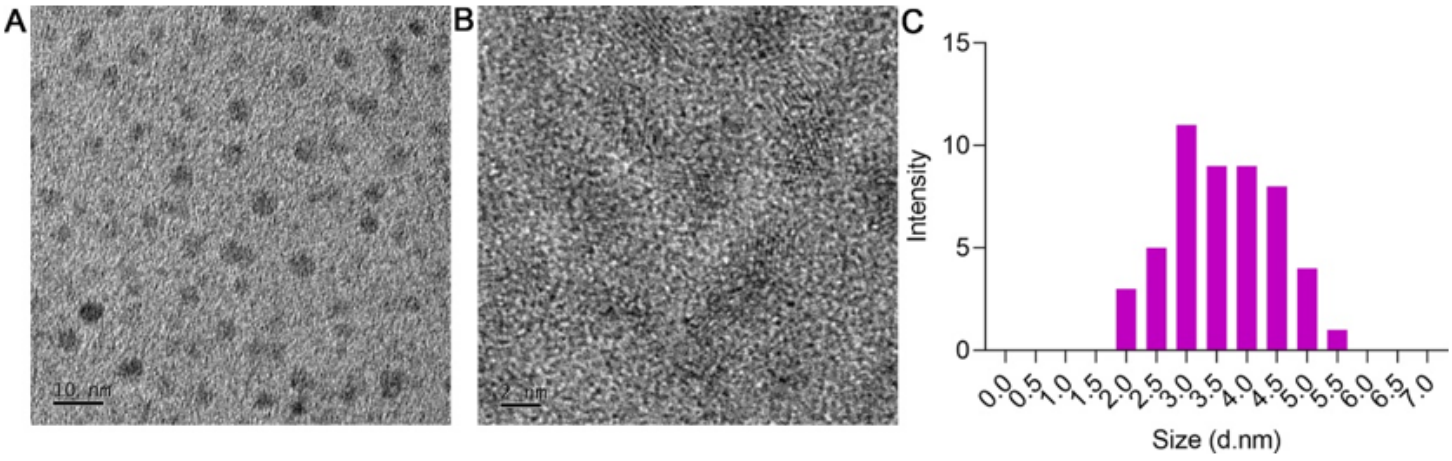

Figure 1

Characterization of GQDs. (A, B) TEM image with different magnification of GQDs. (C) size distribution of GQDs.

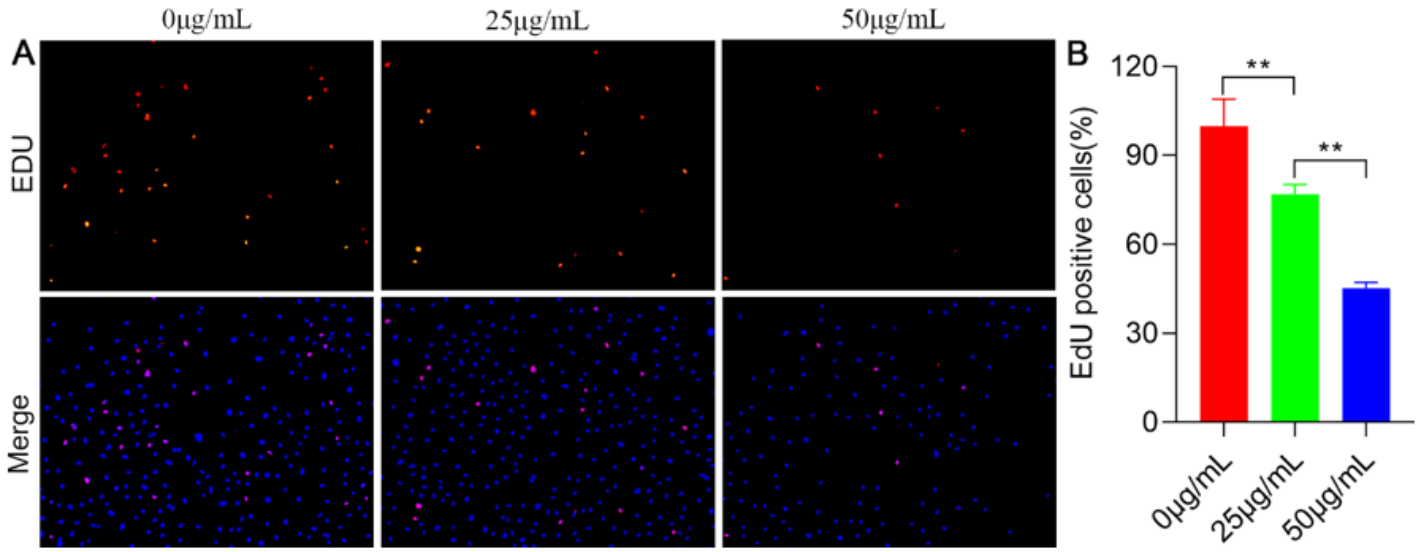

Figure 2

GQDs inhibit HUVECs cell proliferation *in vitro*. (A) GQDs inhibit the proliferation of HUVECs. EdU assay was used to determine cell proliferation. Total cells were stained in blue and proliferating cells were stained in red. (B) quantitative measurements of the percentage of EdU positive cells. Data was presented as the means ± SD, n=4 (**P<0.01; ***P<0.001)

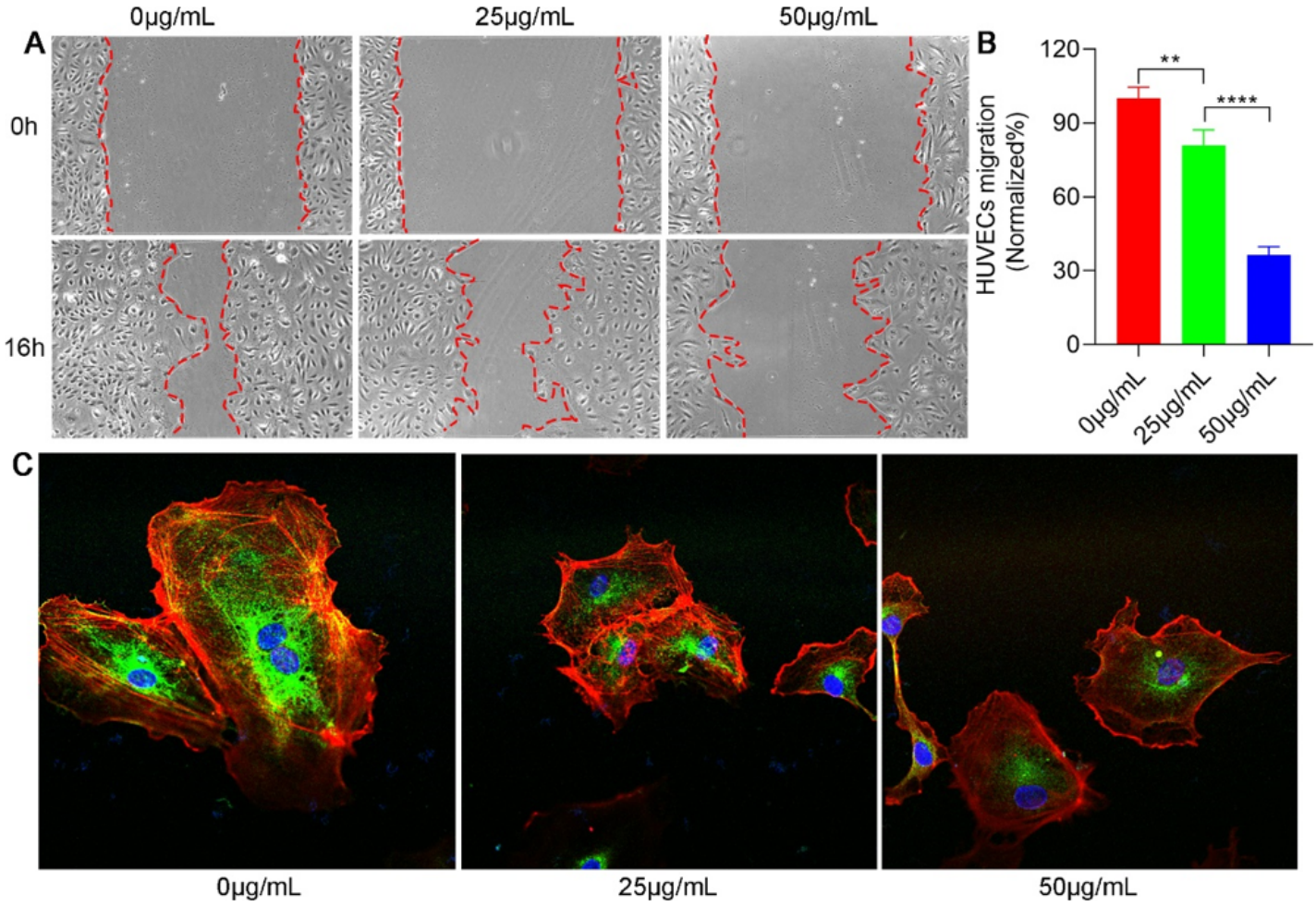

Figure 3

GQDs impair cell migration of HUVECs. (A) Microscopy images of HUVECs treated with GQDs in a cell scratch migration assay. (B) Quantitation of HUVECs migrated distance from the images presented in panel. Error bars represent mean ± SD. *P < 0.05, **P < 0.01. (C) Disruption of cytoskeleton in HUVECs by GQDs. Actin and tubulin were visualized using phalloidin-rhodamine (red) and anti-α-tubulin antibody (green), respectively. Data was presented as the means ± SD, n=4 (**P<0.01; ***P<0.001)

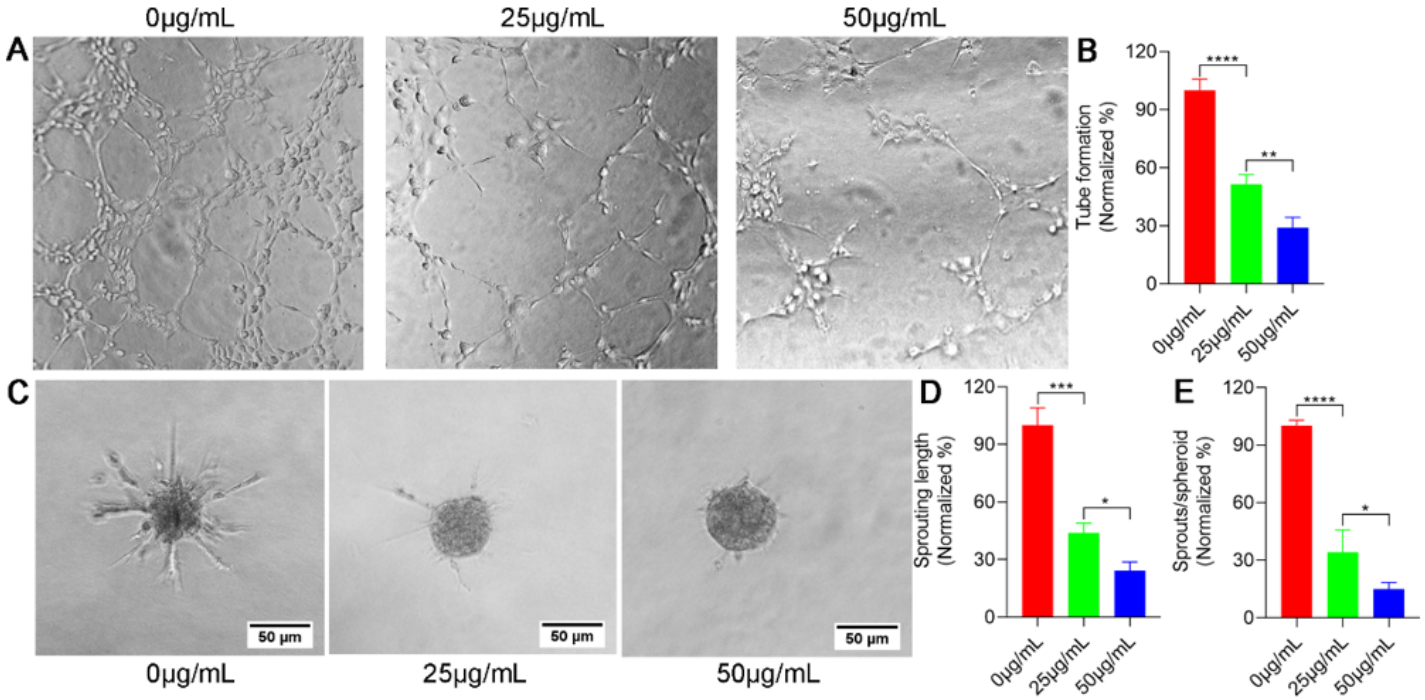

Figure 4

GQDs attenuate tube formation and sprouting of HUVECs. (A) Representative images of GQDs inhibited tube formation of HUVECs. (B) Quantitative of the relative tube formation rate for each group. (C) Representative images of GQDs inhibited angiogenesis in sprouting assay. (D, E) HUVECs sprouting was quantified as sprouting length of HUVECs and sprouts numbers surrounding the spheroid. Error bars represent mean ± SD. *P < 0.05, **P < 0.01.

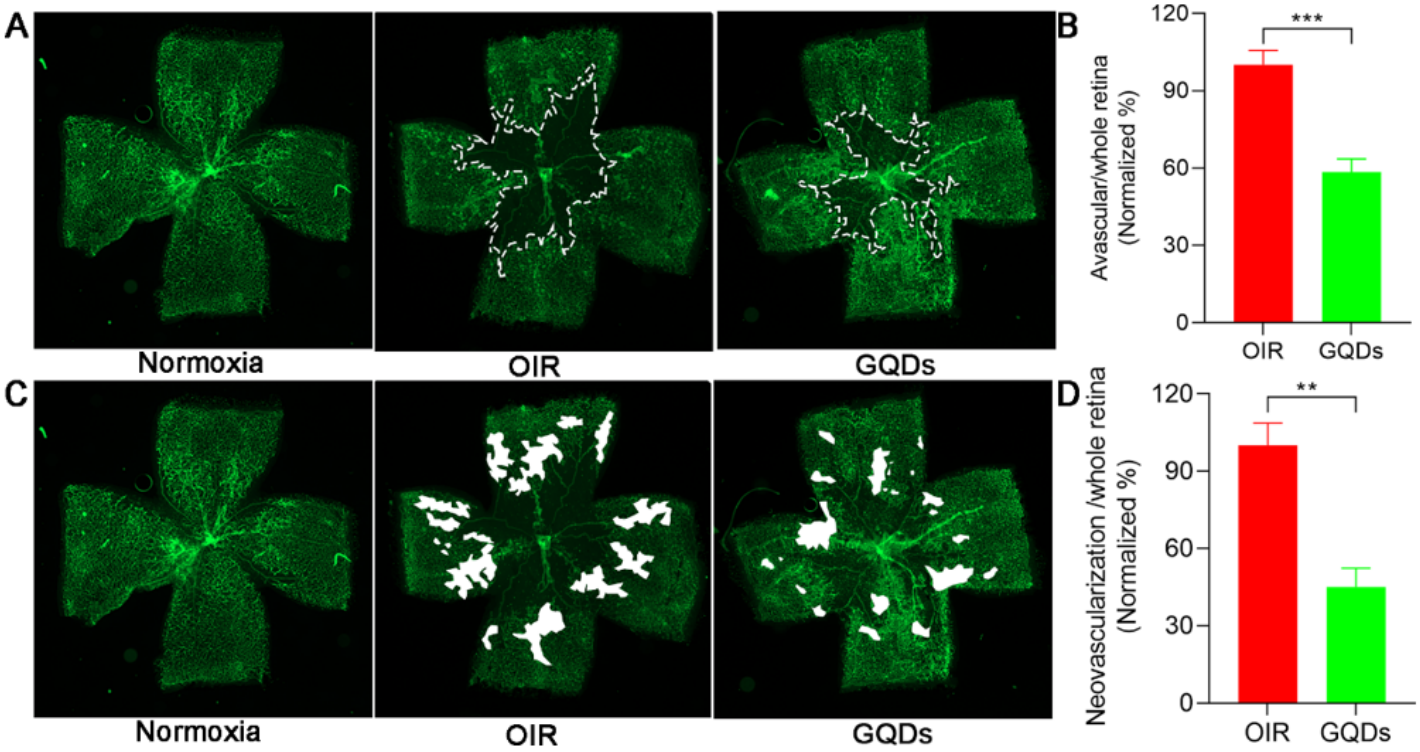

Figure 5

GQDs inhibit retinal angiogenesis in the OIR model. (A) Representative images of the mouse retinas from normal mouse, OIR control group and OIR models injected with GQDs. The white dotted line outlines a vascular area in the central retinal (B) Quantitative analysis of the avascular area in OIR control group and GQDs treated group. Quantitative analysis of the neovascularization area in OIR control group and GQDs treated group. Data was presented as the means ± SD, n=4 (**P<0.01; ***P<0.001)

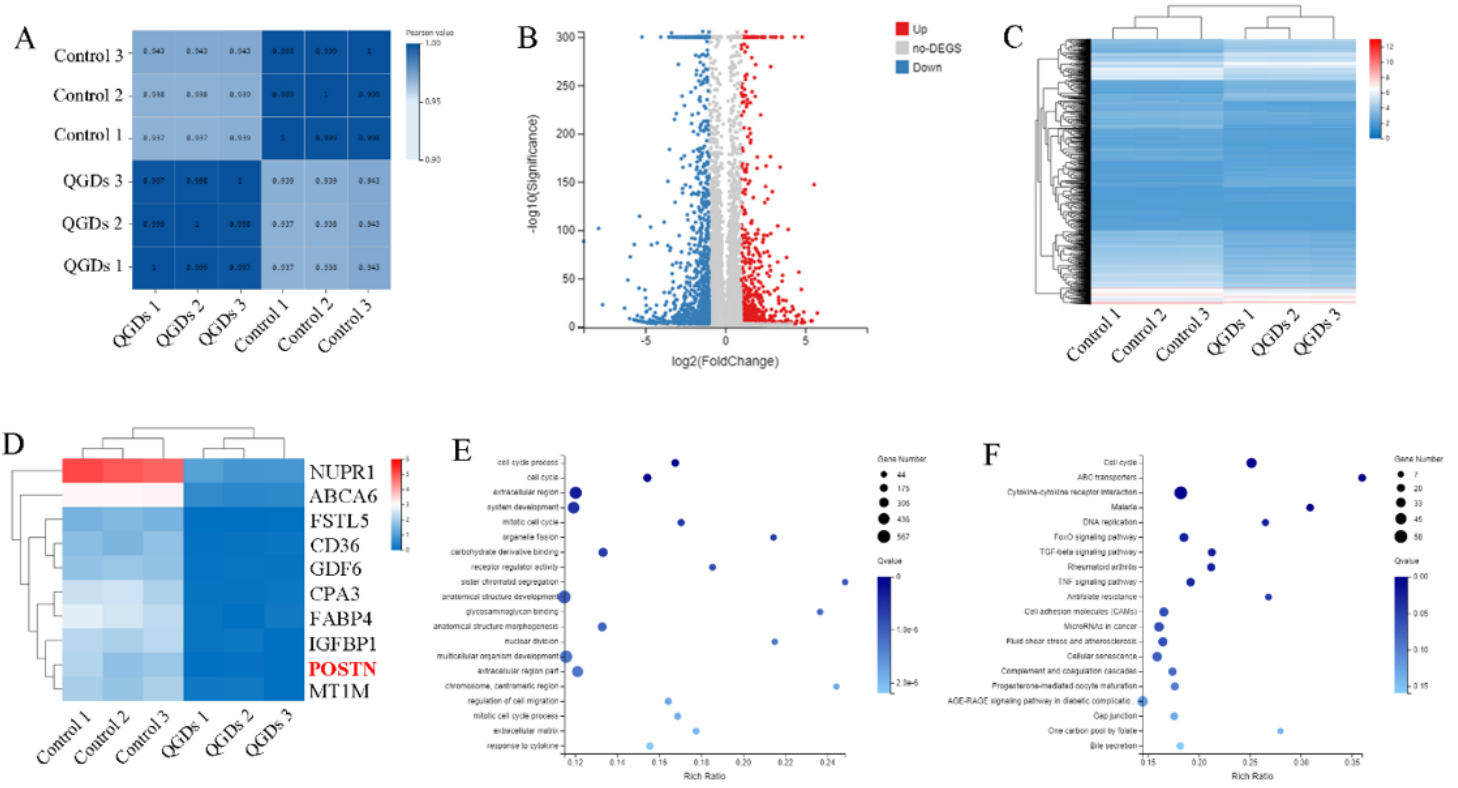

Figure 6

Analysis of gene expression profiles in GQDs treated HUVECs. (A) Pearson correlation coefficient of GQDs groups and control groups. (B) Log2 fold change for GQDs treatment compared to the control. (C) Heatmap of hierarchical clustering of interested genes. Blue and red indicate down-regulation and up-regulation respectively. (D) Heatmap of hierarchical clustering of the top 10 differentially expressed genes. (E) GO categorization of the top 10 differentially expressed genes. (F) KEGG pathway enrichment analysis of the top 10 differentially expressed genes.

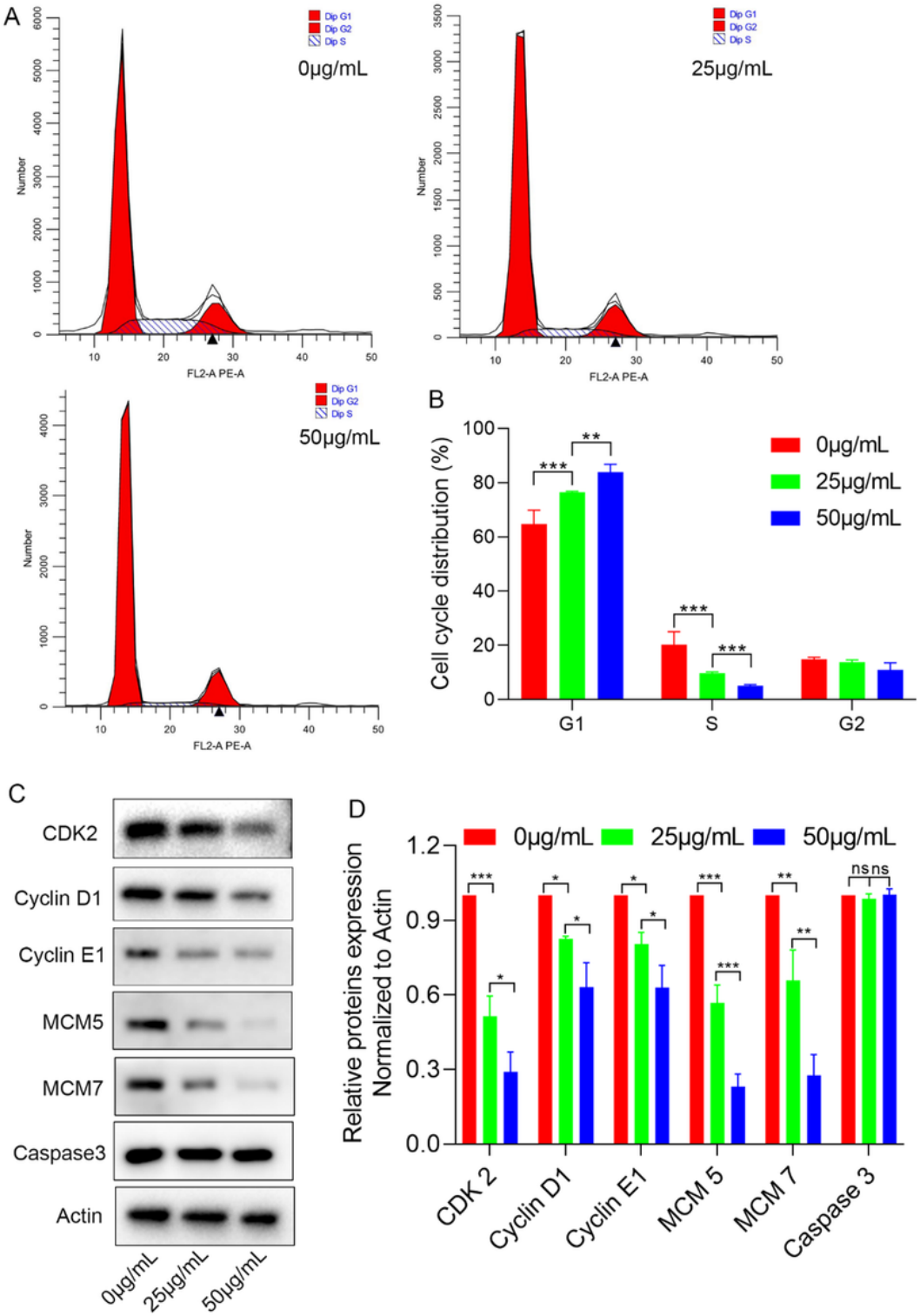

Figure 7

GQDs induce cell cycle arrest in G1 phase. (A) Representative images of HUVECs cell cycle distribution in the control group and GQDs group. (B) Quantitative analysis of cell cycle distribution. Data was presented as the means ± SD, n=3 (**P<0.01; ***P<0.001). (C) Electrophoresis results of the cell cycle-related proteins, CDK2, Cyclin D1, Cyclin E1, MCM5, MCM7 and Caspase 3. (D) Quantitative analysis of relative proteins expression. Data was presented as the means ± SD, n=3 (*P<0.05, **P<0.01; ***P<0.001).

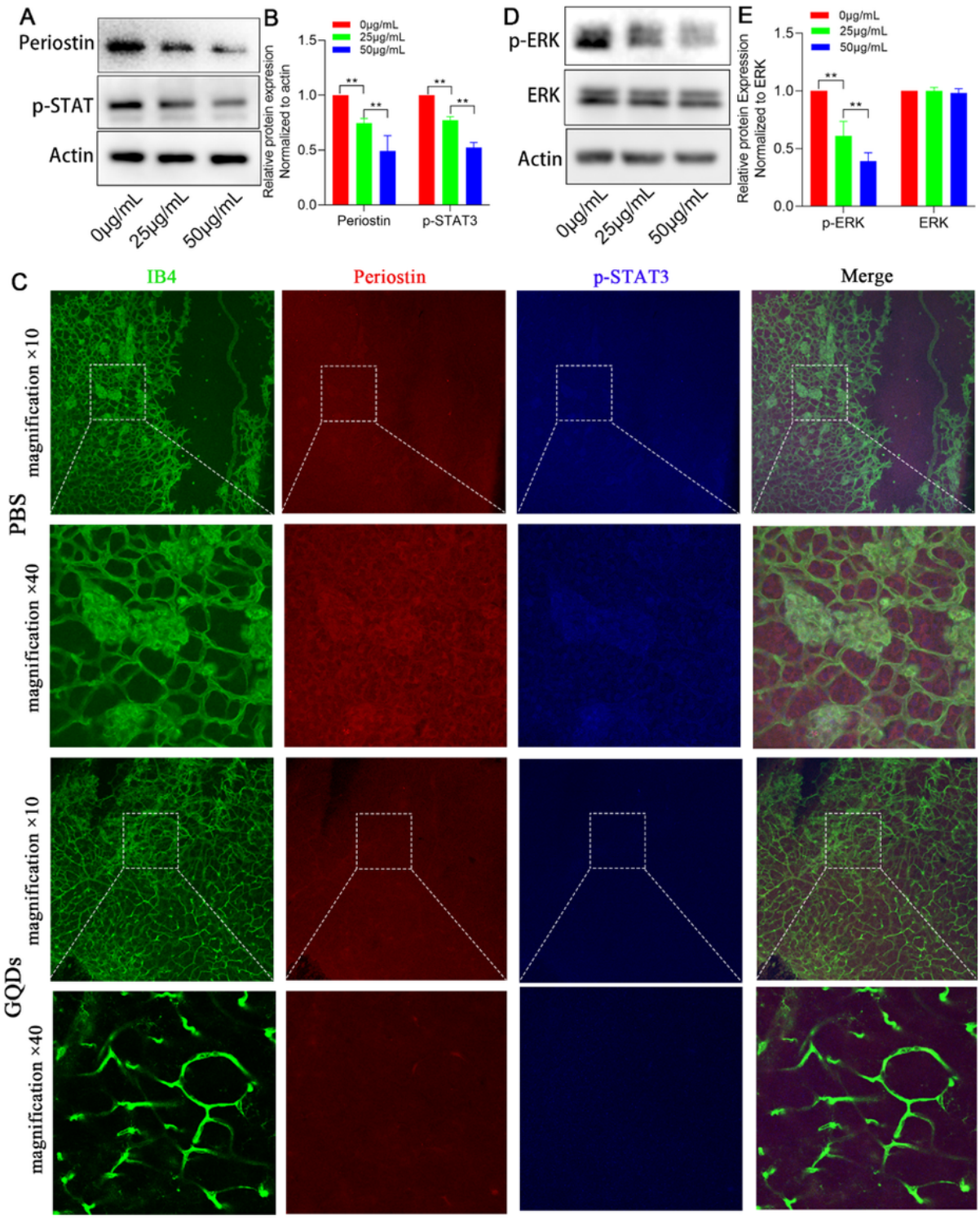

Figure 8

The possible mechanism of GQDs rescued angiogenic retinopathy. (A) GQDs inhibit the expression of periostin by downregulating p-STAT3. (B) Quantitative analysis of relative proteins expression. Data was presented as the means ± SD, n=3 (**P<0.01). (C) Representative confocal images of OIR model retinas after intravitreal injection with PBS and GQDs. Retinas were stained with IB4 (green), periostin(red) and p-

STAT3 (blue). (D) GQDs inhibit the phosphorylation of ERK. (E) Quantitative analysis of relative proteins expression. Data was presented as the means ± SD, n=3 (**P<0.01).

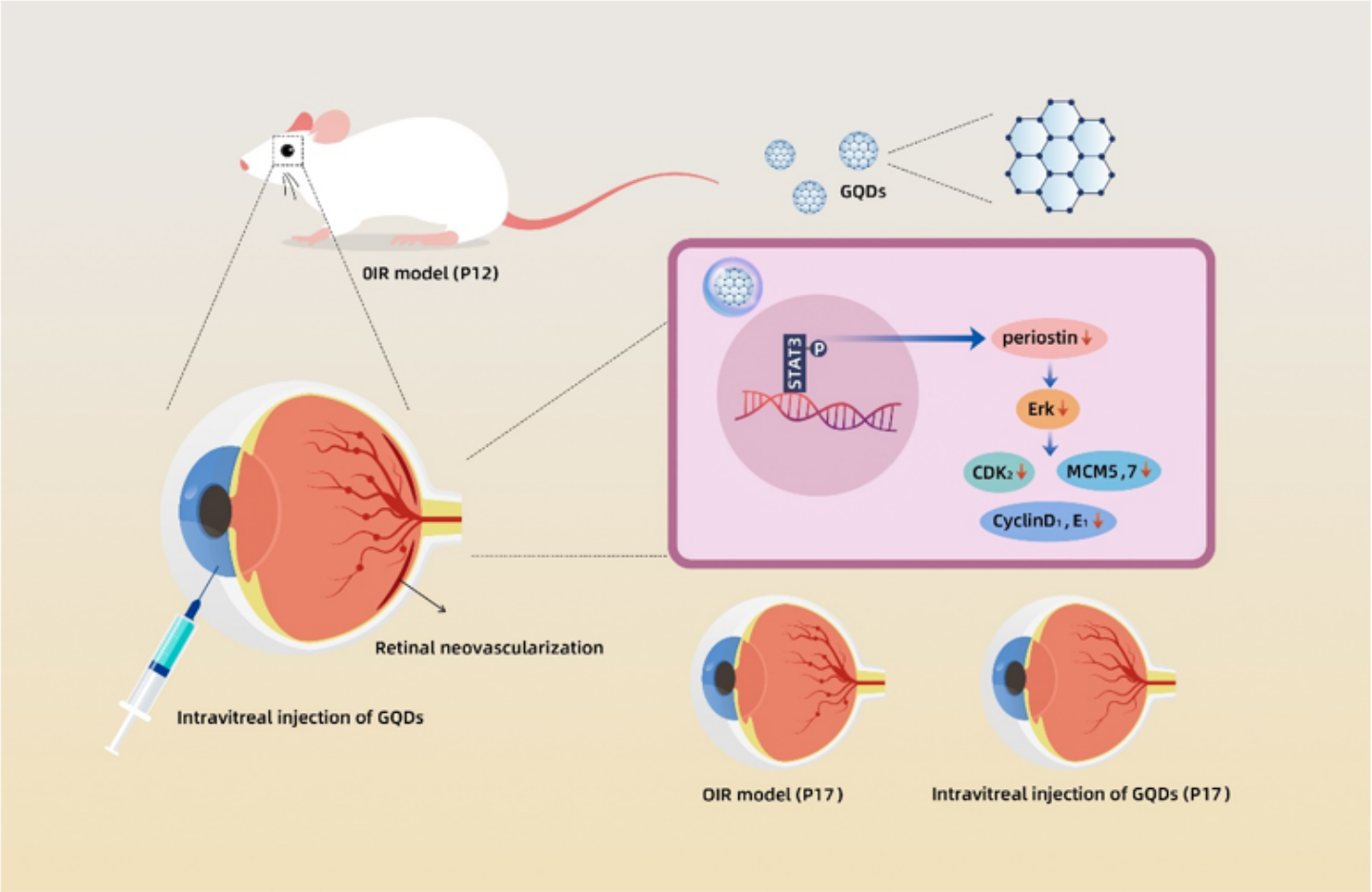

Figure 9

Schematic illustration of the role and mechanism of GQDs rescued angiogenic retinopathy.

Supplementary Files

This is a list of supplementary files associated with this preprint. Click to download.

- Supplementary.docx
- GraphicalAbstract.png